UAV-Enabled Communication Using NOMA

Nasir, A. A., Tuan, H. D., Duong, Q., & Poor, H. V. (2019). UAV-Enabled Communication Using NOMA. *IEEE Transactions on Communications*. https://doi.org/10.1109/TCOMM.2019.2906622

Published in:
IEEE Transactions on Communications

Document Version:
Peer reviewed version

Queen's University Belfast - Research Portal:
Link to publication record in Queen's University Belfast Research Portal

Publisher rights
Copyright 2019, Institute of Electrical and Electronics Engineers.
This work is made available online in accordance with the publisher's policies. Please refer to any applicable terms of use of the publisher.

General rights
Copyright for the publications made accessible via the Queen's University Belfast Research Portal is retained by the author(s) and / or other copyright owners and it is a condition of accessing these publications that users recognise and abide by the legal requirements associated with these rights.

Take down policy
The Research Portal is Queen's institutional repository that provides access to Queen's research output. Every effort has been made to ensure that content in the Research Portal does not infringe any person's rights, or applicable UK laws. If you discover content in the Research Portal that you believe breaches copyright or violates any law, please contact openaccess@qub.ac.uk.

Download date:28. Aug. 2022

UAV-Enabled Communication Using NOMA

A. A. Nasir, H. D. Tuan, T. Q. Duong and H. V. Poor

***Abstract*—Unmanned aerial vehicles (UAVs) can be deployed as flying base stations (BSs) to leverage the strength of line-of-sight connections and effectively support the coverage and throughput of wireless communication. This paper considers a multiuser communication system, in which a single-antenna UAV-BS serves a large number of ground users by employing non-orthogonal multiple access (NOMA). The max-min rate optimization problem is formulated under total power, total bandwidth, UAV altitude, and antenna beamwidth constraints. The objective of max-min rate optimization is non-convex in all optimization variables, i.e. UAV altitude, transmit antenna beamwidth, power allocation and bandwidth allocation for multiple users. A path-following algorithm is proposed to solve the formulated problem. Next, orthogonal multiple access (OMA) and dirty paper coding (DPC)-based max-min rate optimization problems are formulated and respective path-following algorithms are developed to solve them. Numerical results show that NOMA outperforms OMA and achieves rates similar to those attained by DPC. In addition, a clear rate gain is observed by jointly optimizing all the parameters rather than optimizing a subset of parameters, which confirms the desirability of their joint optimization.**

***Index Terms*—Unmanned aerial vehicle (UAV), non-orthogonal multiple access (NOMA), orthogonal multiple access (OMA), dirty paper coding (DPC), non-convex optimization, throughput.**

I. Introduction

Unmanned aerial vehicles (UAVs) can assist normal communication networks by acting as flying base stations (UAV-BSs) and taking care of traffic demand in exceptional situations, e.g., sports events, concerts, disaster position, military situations, traffic congestion, etc. [1]–[6]. UAVs can also function as temporary hotspots or relay nodes for connections between the safe area and disaster areas [7]–[9]. Ground users served by the UAV-BSs can expect line-of-sight (LoS) air-to-ground communication. Thus, UAV-enabled communication can be efficient in supporting the coverage and throughput of wireless communications [10], [11].

UAV-enabled communication networks have recently gained significant interests and are actively investigated in open literature. Thanks to the flexibility of UAV deployment, the coverage area, throughput, and energy efficiency of UAV-enabled communication can be improved by optimizing different parameters, such as, UAV placement or UAV trajectory design [12]–[15], considering multiple-UAV setup [16], [17], beamwidth control [18], power allocation [19], joint power allocation and UAV placement optimization [1], [20], joint bandwidth allocation and trajectory design [21], or joint bandwidth and power allocation [22].

Unlike conventional cellular communication, which operates in a rich scattering environment that supports multi-antenna array transmission for spatial diversity, UAV-enabled downlink communication exhibits much poorer scattering and as such a single-antenna UAV is most desired. To be served by the same UAV over the same time, multiple users must share the communication bandwidth. Usually each user is assigned an individual bandwidth channel so its achievable rate is very sensitive to the number of users sharing the same bandwidth. Naturally one may think to assign a bandwidth channel to a group users but this would be not efficient because it is conventionally known that over the same transmission bandwidth, the downlink communication is only efficient when the number of transmit antennas is not less than the number of served users. Meanwhile, non-orthogonal multiple access (NOMA) is known to simultaneously serve multiple users in non-orthogonal resources, by separating the users in the power domain [23], [24]. NOMA can improve the achievable rate of far users (who receive lower received signal power) by allowing the near-by users (who receive higher received signal power) to access the information intended for the far users [25], [26].

There are quite a few recent studies that have considered the use of NOMA to improve the performance of UAV-enabled communication system. In [27], the authors considered a UAV-BS to communicate with two ground users using NOMA and investigated their outage probability. In [28], the authors characterized the capacity region of a UAV-enabled broadcast channel with two ground users and jointly optimized the UAVs trajectory and transmit power/rate allocations over time. In [29], the authors considered a multi-antenna UAV-BS to generate directional

This work was supported by the KFUPM Research Project #SB171005, in part by Institute for Computational Science and Technology, Hochiminh city, Vietnam, in part by the Australian Research Council's Discovery Projects under Project DP190102501, in part by the U.K. Royal Academy of Engineering Research Fellowship under Grant RF1415\14\22, and in part by U.S. National Science Foundation under Grants CCF-093970 and CCF-1513915

Ali A. Nasir is with the Department of Electrical Engineering, King Fahd University of Petroleum and Minerals (KFUPM), Dhahran, Saudi Arabia (email: anasir@kfupm.edu.sa).

Hoang D. Tuan is with the School of Electrical and Data Engineering, University of Technology Sydney, Broadway, NSW 2007, Australia (email: Tuan.Hoang@uts.edu.au).

Trung Q. Duong is with Queen's University Belfast, Belfast BT7 1NN, UK (email: trung.q.duong@qub.ac.uk)

H. Vincent Poor is with the Department of Electrical Engineering, Princeton University, Princeton, NJ 08544, USA (email: poor@princeton.edu).

beams and served multiple users to maximize their outage sum rates by using NOMA and beam scanning. In [30], the authors employed a UAV system and NOMA to optimize power allocation and UAV altitude to maximize sum-rate for two users [30]. However, in order to achieve the maximum rate gains from UAV-enabled communication, it is important to jointly optimize multiple relevant parameters, e.g., UAV altitude, antenna beamwidth, power allocation and bandwidth allocation. To the best authors' knowledge, this important problem, with a NOMA setting, is still unsolved.

In this article, we consider a multiuser communication system, in which a single-antenna UAV-BS serves a large number of ground users by employing NOMA. Our work is novel and contributive in the following aspects:

- Unlike previous works, we jointly optimize multiple parameters, e.g., the UAV's flying altitude, transmit antenna beamwidth, and the amount of power and bandwidth allocated to multiple users, and show the performance benefit achieved due to this joint optimization. Our objective is to solve the max-min rate optimization problem under total power, total bandwidth, UAV altitude and antenna beamwidth constraints. The objective function is non-convex in all optimization variables, i.e., power, bandwidth, altitude, and beamwidth. In addition, it is also challenging to handle the coverage constraint, which is dependent nonlinearly on the beamwidth and UAV altitude. We tackle these challenges by using inner convex approximations and propose a path-following algorithm to solve the problem.
- We also formulate orthogonal multiple access (OMA) and dirty paper coding (DPC)-based max-min rate optimization problems and develop path-following algorithms to solve them.
- Numerical results show that NOMA outperforms OMA and achieves rates similar to those attained by DPC. In addition, we observe a clear rate gain by jointly optimizing all the parameters rather than optimizing subset of parameters, which emphasize the need of their joint optimization.

Organization: The paper is organized as follows. Section II presents the formulation of max-min rate optimization problems. Section III describes algorithms to solve the formulated problems. Section IV evaluates the performance of our proposed algorithms using numerical examples. Finally, Section V concludes the paper.

II. System Model and Problem Statement

Let us consider that a certain out-door location (stadium, traffic jam, concert, etc.) is served by a single-antenna UAV as depicted in Fig. 1. We assume that there are K ground users in the location, such that $K/2$ users, $k \in \{1, \ldots, K/2\}$, are located in closer vicinity (in terms of Euclidean distance) of the UAV, and are called "near users" or "cell-centered users". The remaining $K/2$ users, $k \in \{K/2+1, \ldots, K\}$ are located relatively at farther distances, and are called "far users" or "cell-edge users". The UAV can employ NOMA to pair each near user with each of the far users.

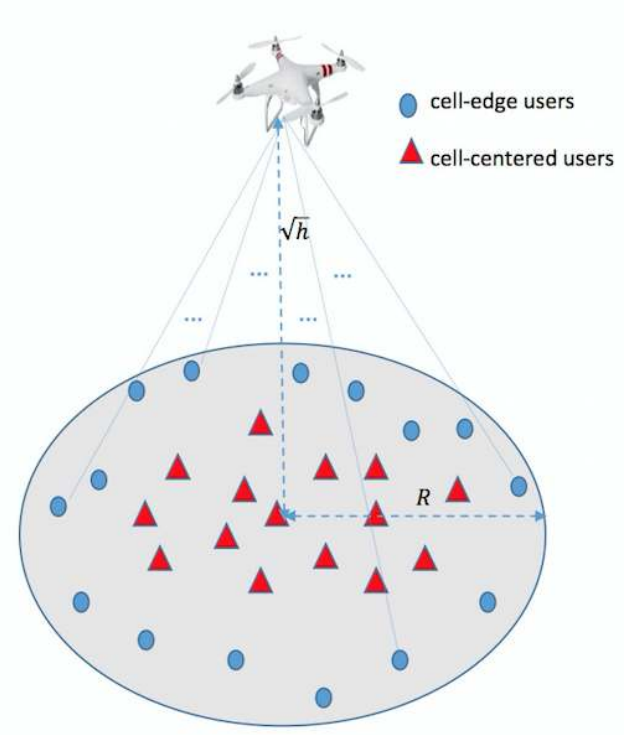

Fig. 1. A system model showing UAV-BS and the ground users.

Let θ be the squared antenna beamwidth, h be the squared UAV altitude (or UAV height above ground), which must satisfy the coverage condition

$$R \leq \sqrt{h} \tan \sqrt{\theta}, \tag{1}$$

where R is the radius of the coverage, so all users are located inside the coverage area. Note that we have to use $\sqrt{h}$ and $\sqrt{\theta}$ for the UAV altitude and its antenna beamwidth, respectively, as it will later on simplify the handling of the non-convex coverage constraint (1). Let g_o denote the channel power gain at a reference distance of 1 m, $z_k = (x_k, y_k)$ denote the coordinates of user k and $z_u = (x_u, y_u)$ denote the location of the UAV projected on the horizontal ground plane. The channel power gain between the UAV and user k is given by

$$\begin{aligned} \hbar_k(h,\theta) &= \frac{g_o |\tilde{h}_k|^2}{\theta(\|z_k - z_u\|^2 + h)^{\alpha/2}} \\ &= \frac{g_o \tilde{g}_k}{\theta(\|z_k - z_u\|^2 + h)^{\alpha/2}} \end{aligned} \tag{2}$$

where α is the path-loss exponent and $\tilde{h}_k \sim \mathcal{CN}(\mu, 2\sigma^2)$, represents the Rician distributed small scale fading channel co-efficient with Rician factor $K_R = |\mu|^2/2\sigma^2$ and normal-

ized power $\mathbb{E}(|\tilde{h}_k|^2) = 1$ [9], or in other words, $\tilde{g}_k \equiv |\tilde{h}_k|^2$ follows non-central chi-square distribution [31].

Let $\mathcal{B}$ be the total available bandwidth, which can be optimally divided among the near-by users $k \in \{1, \ldots, K/2\}$, such that the bandwidth allocated for user k can be written as

$$w_k = \tau_k \mathcal{B}, \quad k \in \{1, \ldots, K/2\}, \tag{3}$$

where $0 \leq \tau_k \leq 1$ is the fraction of the bandwidth allocated to the user k. Accordingly, each near-by user k is "assigned" a far-user $j(k) = k + \frac{K}{2}$ to share the bandwidth w_k. In this work, we have simply paired the near-by user with the far-user on the basis of the minimum Euclidean distance.[1]

There are a couple of transmission techniques to improve the multi-user rates. In the following, we will formulate the multi-user rate max-min optimization problem for NOMA, DPC, and OMA.

A. NOMA Problem Formulation

To make the rate functions more appealing, we use (2) and introduce

$$d_k = \|z_k - z_u\|^2, k = 1, \ldots, K.$$

NOMA allows user k to decode the information intended for the paired user $j(k)$ to cancel the user $j(k)$'s interference in decoding the information intended for it. Assuming additive white Gaussian noise (AGWN) channel, the achievable rate in nats/sec/Hz of user $k \in \{1, 2, \ldots, K/2\}$, is given by

$$\begin{aligned} r_k(\boldsymbol{\tau}, \mathbf{p}, h, \theta) &= \tau_k \ln\left(1 + \frac{p_k \hbar_k(h,\theta)}{\sigma_B \tau_k}\right) \\ &= \tau_k \ln\left(1 + \frac{g_o \tilde{g}_k p_k}{\sigma_B \tau_k \theta (d_k + h)^{\alpha/2}}\right), \end{aligned} \tag{4}$$

where $\sigma_B = \sigma^2 \mathcal{B}$ with the noise power density σ^2, so $\sigma_B \tau_k$ is the noise power over the bandwidth $\tau_k \mathcal{B}$, p_k is the power of signal carrying the information intended for it, $\boldsymbol{\tau} \triangleq (\tau_1, \ldots, \tau_{K/2})$, and $\mathbf{p} \triangleq (p_1, \ldots, p_K)$.

The achievable rate of user $j(k)$ in nats/sec/Hz is given by

$$r_{j(k)}(\boldsymbol{\tau}, \mathbf{p}, h, \theta) = \min\left\{r^1_{j(k)}(\boldsymbol{\tau}, \mathbf{p}, h, \theta), r^2_{j(k)}(\boldsymbol{\tau}, \mathbf{p}, h, \theta)\right\}, \tag{5}$$

where,

$$\begin{aligned} r^2_{j(k)}(\boldsymbol{\tau}, \mathbf{p}, h, \theta) &= \tau_k \ln\left(1 + \frac{p_{j(k)} \hbar_{j(k)}(h,\theta)}{\sigma_B \tau_k + p_k \hbar_{j(k)}(h,\theta)}\right) \\ &= \tau_k \ln\left(1 + \frac{g_o \tilde{g}_{j(k)} p_{j(k)}}{\sigma_B \tau_k \theta (d_{j(k)} + h)^{\alpha/2} + g_o \tilde{g}_{j(k)} p_k}\right), \end{aligned} \tag{6}$$

[1]The more sophisticated user-pairing strategies may improve the performance of NOMA networks (see e.g., [32]). Finding an optimum pairing strategy is out of scope of this work. However, our simulation results in Section IV clearly shows the performance gains of our proposed Algorithms, even with our simple pairing strategy.

is the rate by user $j(k)$, $k \in \{1, 2, \ldots, K/2\}$, in decoding its own message, and

$$\begin{aligned} r^1_{j(k)}(\boldsymbol{\tau}, \mathbf{p}, h, \theta) &= \tau_k \ln\left(1 + \frac{p_{j(k)} \hbar_k(h,\theta)}{\sigma_B \tau_k + p_k \hbar_k(h,\theta)}\right) \\ &= \tau_k \ln\left(1 + \frac{g_o \tilde{g}_k p_{j(k)}}{\sigma_B \tau_k \theta (d_k + h)^{\alpha/2} + g_o \tilde{g}_k p_k}\right), \end{aligned} \tag{7}$$

is the rate by user k, $k \in \{1, 2, \ldots, K/2\}$, in decoding the user $j(k)$'s message.

The optimization problem is to find the optimal values of bandwidth allocation $\boldsymbol{\tau}$, power allocation $\mathbf{p}$, UAV altitude $\sqrt{h}$, and antenna beamwidth $\sqrt{\theta}$, with the objective of maximizing the worst user's rate. It can be formulated mathematically as follows:

$$\max_{\boldsymbol{\tau}, \mathbf{p}, h, \theta} f^{\text{NOMA}}(\boldsymbol{\tau}, \mathbf{p}, h, \theta) \triangleq \min_{k=1,\ldots,K} r_k^{\text{NOMA}}(\boldsymbol{\tau}, \mathbf{p}, h, \theta) \tag{8a}$$

$$\text{s.t. } (1),$$

$$h^2_{\min} \leq h \leq h^2_{max}, \theta^2_{\min} \leq \theta \leq \theta^2_{\max}, \tag{8b}$$

$$\sum_{k=1}^{K/2} \tau_k = 1, \ \& \ \tau_k \geq 0, \ \forall k \in \{1, \ldots, K/2\} \tag{8c}$$

$$\sum_{k=1}^{K} p_k = P, \ \& \ \ p_k \geq 0, \ \forall k \in \{1, \ldots, K\}, \tag{8d}$$

where

$$r_k^{\text{NOMA}}(\boldsymbol{\tau}, \mathbf{p}, h, \theta) = \begin{cases} r_k(\boldsymbol{\tau}, \mathbf{p}, h, \theta), & k \in \{1, \ldots, K/2\}, \\ r_{j(k)}(\boldsymbol{\tau}, \mathbf{p}, h, \theta), & j(k) \in \{K/2+1, \ldots, K\}, \end{cases}$$

$r_k(\boldsymbol{\tau}, \mathbf{p}, h, \theta)$ is given by (4), $r_{j(k)}(\boldsymbol{\tau}, \mathbf{p}, h, \theta)$ is given by (5), P is the total power budget, and $\theta_{\min}$ and $\theta_{\max}$ specify the allowed range of the antenna beamwidth, i.e., $(0, \pi/2)$. It is quite challenging to solve the non-convex problem (8) because the objective function (8a) is non-convex and non-linear function of four different types of variables, i.e., power, bandwidth, altitude, and beamwidth. In addition, it is also challenging to handle the coverage constraint, which is dependent nonlinearly on the beamwidth and UAV altitude. In Section III, we will provide an inner convex approximation-based path-following algorithm to solve this problem.

B. DPC Problem Formulation

For two users sharing the same bandwidth, the capacity-achieving DPC is practical [33]–[35]. In DPC, the users' data is successively decoded in a specific order. Thus, under DPC, cell-centered user k perfectly eliminates the interfering signal intended for user $j(k)$ from its received signal. Therefore, the rate of user $k \in \{1, \ldots, K/2\}$ is defined by (4) while the rate of user $j(k) \in \{K/2+1, \ldots, K\}$ is

defined by (6) [26]. Thus, the max-min rate optimization problem under DPC can be formulated as follows:

$$\max_{\boldsymbol{\tau},\mathbf{p},h,\theta} f^{\text{DPC}}(\boldsymbol{\tau},\mathbf{p},h,\theta) \triangleq \min_{k=1,\ldots,K} r_k^{\text{DPC}}(\boldsymbol{\tau},\mathbf{p},h,\theta) \quad \text{s.t.} \quad (1),(8b)-(8d), \tag{9}$$

where

$$r_k^{\text{DPC}}(\boldsymbol{\tau},\mathbf{p},h,\theta) = \begin{cases} r_k(\boldsymbol{\tau},\mathbf{p},h,\theta), & k \in \{1,\ldots,K/2\}, \\ r^2_{j(k)}(\boldsymbol{\tau},\mathbf{p},h,\theta), & j(k) \in \{K/2+1,\ldots,K\}, \end{cases}$$

$r_k(\boldsymbol{\tau},\mathbf{p},h,\theta)$ is given by (4) and far-user rate $r^2_{j(k)}(\boldsymbol{\tau},\mathbf{p},h,\theta)$ is defined in (6).

C. OMA Problem Formulation

For OMA, the optimization problem can be formulated in two ways. The first way, which we term "OMA-1" is to allocate distinct bandwidth to all users, i.e., in (3), $w_k = \tau_k \mathcal{B}$, will be defined for $k \in \{1,\ldots,K\}$. Thus, under this OMA-1, the optimization problem can be formulated as follows:

$$\max_{\boldsymbol{\tau},\mathbf{p},h,\theta} f^{\text{OMA-1}}(\boldsymbol{\tau},\mathbf{p},h,\theta) \triangleq \min_{k=1,\ldots,K} r_k^{\text{OMA-1}}(\boldsymbol{\tau},\mathbf{p},h,\theta) \tag{10a}$$

$$\text{s.t.} \quad (1),(8b),(8d), \quad \sum_{k=1}^{K} \tau_k = 1, \ \& \ \tau_k \geq 0, \ \forall \ k \in \{1,\ldots,K\}, \tag{10b}$$

where $\boldsymbol{\tau} \triangleq (\tau_1,\ldots,\tau_K)$ for OMA-1, $r_k^{\text{OMA-1}}(\boldsymbol{\tau},\mathbf{p},h,\theta) = r_k(\boldsymbol{\tau},\mathbf{p},h,\theta), \ \forall \ k = \{1,\ldots,K\}$ and $r_k(\boldsymbol{\tau},\mathbf{p},h,\theta)$ is defined in (4).

The second option, which we term "OMA-2", is to find optimal $K/2$ bandwidth partitions along with optimal altitude, power, and antenna beamwidth, and solve the following optimization problem:

$$\max_{\boldsymbol{\tau},\mathbf{p},h,\theta} f^{\text{OMA-2}}(\boldsymbol{\tau},\mathbf{p},h,\theta) \triangleq \min_{k=1,\ldots,K/2} r_k^{\text{OMA-2}}(\boldsymbol{\tau},\mathbf{p},h,\theta) \quad \text{s.t.} \quad (1),(8b)-(8d), \tag{11}$$

where

$$r_k^{\text{OMA-2}}(\boldsymbol{\tau},\mathbf{p},h,\theta) = \begin{cases} r_k^{\text{O}}(\boldsymbol{\tau},\mathbf{p},h,\theta), & k \in \{1,\ldots,K/2\}, \\ r^{\text{O}}_{j(k)}(\boldsymbol{\tau},\mathbf{p},h,\theta), & j(k) \in \{K/2+1,\ldots,K\}, \end{cases}$$

such that

$$r_k^{\text{O}}(\boldsymbol{\tau},\mathbf{p},h,\theta) = \tau_k \ln\left(1+\frac{p_k \hbar_k(h,\theta)}{\sigma_B \tau_k + p_{j(k)}\hbar_k(h,\theta)}\right) = \tau_k \ln\left(1+\frac{g_o \tilde{g}_k p_k}{\sigma_B \tau_k \theta (d_k+h)^{\alpha/2} + g_o \tilde{g}_k p_{j(k)}}\right), \quad \forall \ k \in \{1,\ldots,K/2\}, \tag{12a}$$

$$r^{\text{O}}_{j(k)}(\boldsymbol{\tau},\mathbf{p},h,\theta) = \tau_k \ln\left(1+\frac{p_{j(k)} \hbar_{j(k)}(h,\theta)}{\sigma_B \tau_k + p_k \hbar_{j(k)}(h,\theta)}\right) = \tau_k \ln\left(1+\frac{g_o \tilde{g}_{j(k)} p_{j(k)}}{\sigma_B \tau_k \theta (d_{j(k)}+h)^{\alpha/2} + g_o \tilde{g}_{j(k)} p_k}\right), \quad \forall \ j(k) \in \{K/2,\ldots,K\}. \tag{12b}$$

Since user k and user $j(k)$ are sharing the bandwidth, user k experiences interference from user $j(k)$ in (12a) to decode its own data and user $j(k)$ experiences interference from user k in (12b) to decode its own data.

III. Algorithms

In this section, we will solve the formulated problems in Section II, which are non-convex optimization problems and thus pose computational challenges. In this section, we will be using the following Lemma.

Lemma 1: For every $x > 0$, $y > 0$, $\tau > 0$, $\bar{x} > 0$, $\bar{y} > 0$ and $\bar{\tau} > 0$:

$$\tau \ln\left(1+\frac{1}{xy}\right) \geq 2\bar{\tau}\ln\left(1+\frac{1}{\bar{x}\bar{y}}\right) + \frac{\bar{\tau}\left(2-x/\bar{x}-y/\bar{y}\right)}{1+\bar{x}\bar{y}} - \frac{\bar{\tau}^2 \ln(1+1/\bar{x}\bar{y})}{\tau} \tag{13}$$

Proof: See Appendix A.

A. NOMA Algorithm

From the definitions (4) and (6), one can see that the objective function (8a) of the optimization problem (8) is a complex non-concave function. Also, the constraint (1) is non-convex. To obtain a path-following computational procedure [36], [37], which improves a feasible point of (8) after each iteration and converges to an optimal solution, we need to develop a lower-bounding concave approximation for the objective function and also an inner convex approximation for constraint (1).

Let $(\boldsymbol{\tau}^{(\kappa)},\mathbf{p}^{(\kappa)},h^{(\kappa)},\theta^{(\kappa)})$ be a feasible point for (8) that is found at the $(\kappa-1)$th iteration. With regard to the function r_k in (8), applying the inequality (13) in Lemma 1 for

$$\tau = \tau_k, x = \sigma_B \theta / g_o \tilde{g}_k p_k, y = \tau_k (d_k+h)^{\alpha/2}$$

and

$$\bar{\tau} = \tau_k^{(\kappa)}, \bar{x} = \sigma_B \theta^{(\kappa)} / g_o \tilde{g}_k p_k^{(\kappa)}, \bar{y} = \tau_k^{(\kappa)} (d_k + h^{(\kappa)})^{\alpha/2}$$

yields

$$r_k(\boldsymbol{\tau},\mathbf{p},h,\theta) \geq a_k^{(\kappa)} + b_k^{(\kappa)}\left(2 - \frac{p_k^{(\kappa)}}{\theta^{(\kappa)}}\frac{\theta}{p_k} - \frac{\tau_k(d_k+h)^{\alpha/2}}{\tau_k^{(\kappa)}(d_k+h^{(\kappa)})^{\alpha/2}}\right) - \frac{c_k^{(\kappa)}}{\tau_k} \quad (14)$$

where

$$\begin{aligned} 0 < a_k^{(\kappa)} &= 2\bar{\tau}\ln(1+1/\bar{x}\bar{y}),\\ 0 < b_k^{(\kappa)} &= \frac{\bar{\tau}}{1+\bar{x}\bar{y}},\\ 0 < c_k^{(\kappa)} &= \bar{\tau}^2\ln(1+1/\bar{x}\bar{y}). \end{aligned} \quad (15)$$

From (14) it remains to deal with

$$\begin{aligned} \frac{p_k^{(\kappa)}}{\theta^{(\kappa)}}\frac{\theta}{p_k} &= \frac{1}{4}\left(\left(\frac{\theta}{\theta^{(\kappa)}} + \frac{p_k^{(\kappa)}}{p_k}\right)^2 - \left(\frac{\theta}{\theta^{(\kappa)}} - \frac{p_k^{(\kappa)}}{p_k}\right)^2\right)\\ &\leq \frac{1}{4}\left(\frac{\theta}{\theta^{(\kappa)}} + \frac{p_k^{(\kappa)}}{p_k}\right)^2\\ &\triangleq \pi_k^{(\kappa)}(\theta,p_k) \end{aligned} \quad (16)$$

and

$$\begin{aligned} \frac{\tau_k(d_k+h)^{\alpha/2}}{\tau_k^{(\kappa)}(d_k+h^{(\kappa)})^{\alpha/2}} &= \frac{1}{4}\left(\left(\frac{\tau_k}{\tau_k^{(\kappa)}} + \frac{(d_k+h)^{\alpha/2}}{(d_k+h^{(\kappa)})^{\alpha/2}}\right)^2 - \left(\frac{\tau_k}{\tau_k^{(\kappa)}} - \frac{(d_k+h)^{\alpha/2}}{(d_k+h^{(\kappa)})^{\alpha/2}}\right)^2\right)\\ &\leq \frac{1}{4}\left(\frac{\tau_k}{\tau_k^{(\kappa)}} + \frac{(d_k+h)^{\alpha/2}}{(d_k+h^{(\kappa)})^{\alpha/2}}\right)^2\\ &\triangleq \varphi_k^{(\kappa)}(\tau_k,h), \end{aligned} \quad (17)$$

Therefore,

$$r_k(\boldsymbol{\tau},\mathbf{p},h,\theta) \geq r_k^{(\kappa)}(\boldsymbol{\tau},\mathbf{p},h,\theta) \quad (18)$$

for

$$r_k^{(\kappa)}(\boldsymbol{\tau},\mathbf{p},h,\theta) \triangleq a_k^{(\kappa)} + b_k^{(\kappa)}\left(2 - \pi_k^{(\kappa)}(\theta,p_k) - \varphi_k^{(\kappa)}(\tau_k,h)\right) - \frac{c_k^{(\kappa)}}{\tau_k}, \quad (19)$$

which is a concave function under $p_k \geq 0$, as mentioned explicitly in the constraint (8d).

With regard to the function $r_{j(k)}^2$, applying the inequality (13) in Lemma 1 for

$$\begin{aligned} \tau &= \tau_k \quad , \quad x = \sigma_B\theta/g_o\tilde{g}_{j(k)}p_{j(k)},\\ y &= \tau_k(d_{j(k)}+h)^{\alpha/2} + g_o\tilde{g}_{j(k)}p_k/(\sigma_B\theta) \end{aligned}$$

and

$$\begin{aligned} \bar{\tau} &= \tau_k^{(\kappa)} \quad , \quad \bar{x} = \sigma_B\theta^{(\kappa)}/g_o\tilde{g}_{j(k)}p_{j(k)}^{(\kappa)},\\ \bar{y} &= \tau_k^{(\kappa)}(d_{j(k)}+h^{(\kappa)})^{\alpha/2} + g_o\tilde{g}_{j(k)}p_k^{(\kappa)}/(\theta^{(\kappa)}\sigma_B) \end{aligned}$$

yields

$$r_{j(k)}^2(\boldsymbol{\tau},\mathbf{p},h,\theta) \geq a_{j(k)}^{(\kappa)} + b_{j(k)}^{(\kappa)}\left(2 - \frac{p_{j(k)}^{(\kappa)}}{\theta^{(\kappa)}}\frac{\theta}{p_{j(k)}} - \frac{\tau_k(d_{j(k)}+h)^{\alpha/2} + g_o\tilde{g}_{j(k)}p_k/(\sigma_B\theta)}{\tau_k^{(\kappa)}(d_{j(k)}+h^{(\kappa)})^{\alpha/2} + g_o\tilde{g}_{j(k)}p_k^{(\kappa)}/(\sigma_B\theta^{(\kappa)})}\right) - \frac{c_{j(k)}^{(\kappa)}}{\tau_k}, \quad (20)$$

where

$$\begin{aligned} 0 < a_{j(k)}^{(\kappa)} &= 2\bar{\tau}\ln(1+1/\bar{x}\bar{y}),\\ 0 < b_{j(k)}^{(\kappa)} &= \frac{\bar{\tau}}{1+\bar{x}\bar{y}},\\ 0 < c_{j(k)}^{(\kappa)} &= \bar{\tau}^2\ln(1+1/\bar{x}\bar{y}). \end{aligned} \quad (21)$$

From (20), it remains to deal with

$$\begin{aligned} \frac{p_{j(k)}^{(\kappa)}}{\theta^{(\kappa)}}\frac{\theta}{p_{j(k)}} &\leq \frac{1}{4}\left(\frac{p_{j(k)}^{(\kappa)}}{p_{j(k)}} + \frac{\theta}{\theta^{(\kappa)}}\right)^2\\ &\triangleq \pi_{j(k)}^{(\kappa)}(p_{j(k)},\theta), \end{aligned} \quad (22)$$

and

$$\begin{aligned} &\frac{\tau_k(d_{j(k)}+h)^{\alpha/2} + g_o\tilde{g}_{j(k)}p_k/(\sigma_B\theta)}{\tau_k^{(\kappa)}(d_{j(k)}+h^{(\kappa)})^{\alpha/2} + g_o\tilde{g}_{j(k)}p_k^{(\kappa)}/(\sigma_B\theta^{(\kappa)})}\\ &= \frac{(\tau_k/\tau_k^{(\kappa)}).[(d_{j(k)}+h)^{\alpha/2}/(d_{j(k)}+h^{(\kappa)})^{\alpha/2}]}{1 + g_o\tilde{g}_{j(k)}p_k^{(\kappa)}\sigma_B/\theta^{(\kappa)}\tau_k^{(\kappa)}(d_{j(k)}+h^{(\kappa)})^{\alpha/2}}\\ &\quad + \frac{(p_k/p_k^{(\kappa)}).(\theta^{(\kappa)}/\theta)}{\sigma_B\theta^{(\kappa)}\tau_k^{(\kappa)}(d_{j(k)}+h^{(\kappa)})^{\alpha/2}/g_o\tilde{g}_{j(k)}p_k^{(\kappa)} + 1}\\ &\leq \frac{1}{4}\frac{\left((\tau_k/\tau_k^{(\kappa)}) + (d_{j(k)}+h)^{\alpha/2}/(d_{j(k)}+h^{(\kappa)})^{\alpha/2}\right)^2}{1 + g_o\tilde{g}_{j(k)}p_k^{(\kappa)}/\sigma_B\theta^{(\kappa)}\tau_k^{(\kappa)}(d_{j(k)}+h^{(\kappa)})^{\alpha/2}}\\ &\quad + \frac{1}{4}\frac{\left((p_k/p_k^{(\kappa)}) + (\theta^{(\kappa)}/\theta)\right)^2}{\sigma_B\theta^{(\kappa)}\tau_k^{(\kappa)}(d_{j(k)}+h^{(\kappa)})^{\alpha/2}/g_o\tilde{g}_{j(k)}p_k^{(\kappa)} + 1}\\ &\triangleq \nu_k^{(\kappa)}(\tau_k,p_k,\theta). \end{aligned} \quad (23)$$

Therefore,

$$r_{j(k)}^2(\boldsymbol{\tau},\mathbf{p},h,\theta) \geq r_{j(k)}^{2,(\kappa)}(\boldsymbol{\tau},\mathbf{p},h,\theta) \quad (24)$$

for

$$r_{j(k)}^{2,(\kappa)}(\boldsymbol{\tau},\mathbf{p},h,\theta) \triangleq a_{j(k)}^{(\kappa)} + b_{j(k)}^{(\kappa)}\left(2 - \pi_{j(k)}^{(\kappa)}(\theta,p_{j(k)}) - \nu_k^{(\kappa)}(\tau_k,p_k,\theta)\right) - \frac{c_{j(k)}^{(\kappa)}}{\tau_k}. \quad (25)$$

Analogously,

$$r^1_{j(k)}(\boldsymbol{\tau},\mathbf{p},h,\theta) \geq \tilde{a}^{(\kappa)}_{j(k)} + \tilde{b}^{(\kappa)}_{j(k)} \left(2 - \frac{p^{(\kappa)}_{j(k)}}{\theta^{(\kappa)}}\frac{\theta}{p_{j(k)}} - \frac{\tau_k(d_k+h)^{\alpha/2} + g_o\tilde{g}_k p_k/(\sigma_B\theta)}{\tau^{(\kappa)}_k(d_k+h^{(\kappa)})^{\alpha/2} + g_o\tilde{g}_k p^{(\kappa)}_k/(\sigma_B\theta^{(\kappa)})}\right) - \frac{\tilde{c}^{(\kappa)}_{j(k)}}{\tau_k} \geq r^{1,(\kappa)}_{j(k)}(\boldsymbol{\tau},\mathbf{p},h,\theta) \quad (26)$$

for

$$r^{1,(\kappa)}_{j(k)}(\boldsymbol{\tau},\mathbf{p},h,\theta) \triangleq \tilde{a}^{(\kappa)}_{j(k)} + \tilde{b}^{(\kappa)}_{j(k)} \left(2 - \pi^{(\kappa)}_{j(k)}(\theta, p_{j(k)}) - \tilde{\nu}^{(\kappa)}_k(\tau_k, p_k, \theta)\right) - \frac{\tilde{c}^{(\kappa)}_{j(k)}}{\tau_k}, \quad (27)$$

and

$$\tilde{\nu}^{(\kappa)}_k(\tau_k,p_k,\theta) \triangleq \frac{1}{4}\frac{\left((\tau_k/\tau^{(\kappa)}_k) + (d_k+h)^{\alpha/2}/(d_k+h^{(\kappa)})^{\alpha/2}\right)^2}{1+g_o\tilde{g}_k p^{(\kappa)}_k/\sigma_B\theta^{(\kappa)}\tau^{(\kappa)}_k(d_k+h^{(\kappa)})^{\alpha/2}} + \frac{1}{4}\frac{\left((p_k/p^{(\kappa)}_k) + (\theta^{(\kappa)}/\theta)\right)^2}{\sigma_B\theta^{(\kappa)}\tau^{(\kappa)}_k(d_k+h^{(\kappa)})^{\alpha/2}/g_o\tilde{g}_k p^{(\kappa)}_k + 1}, \quad (28)$$

and

$$\begin{aligned}\tilde{a}^{(\kappa)}_{j(k)} &= 2\bar{\tau}\ln(1+1/\bar{x}\bar{y}),\\ \tilde{b}^{(\kappa)}_{j(k)} &= \frac{\bar{\tau}}{1+\bar{x}\bar{y}},\\ \tilde{c}^{(\kappa)}_{j(k)} &= \bar{\tau}^2\ln(1+1/\bar{x}\bar{y}),\end{aligned} \quad (29)$$

under

$$\bar{\tau} = \tau^{(\kappa)}_k \quad , \quad \bar{x} = \sigma_B\theta^{(\kappa)}/g_o\tilde{g}_k p^{(\kappa)}_{j(k)},$$
$$\bar{y} = \tau^{(\kappa)}_k(d_k+h^{(\kappa)})^{\alpha/2} + g_o\tilde{g}_k p^{(\kappa)}_k/(\sigma_B\theta^{(\kappa)}).$$

A lower bounding concave function for the objective function (8a) is

$$f^{\text{NOMA},(\kappa)}(\boldsymbol{\tau},\mathbf{p},h,\theta) = \min_{k=1,\ldots,K} r^{\text{NOMA},(\kappa)}_k(\boldsymbol{\tau},\mathbf{p},h,\theta), \quad (30)$$

where

$$r^{\text{NOMA},(\kappa)}_k(\boldsymbol{\tau},\mathbf{p},h,\theta) = \begin{cases} r^{(\kappa)}_k(\boldsymbol{\tau},\mathbf{p},h,\theta), & k\in\{1,\ldots,K/2\},\\ r^{2,(\kappa)}_{j(k)}(\boldsymbol{\tau},\mathbf{p},h,\theta), & j(k)\in\{K/2+1,\ldots,K\},\end{cases} \quad (31)$$

and

$$r^{(\kappa)}_{j(k)}(\boldsymbol{\tau},\mathbf{p},h,\theta) = \min\left\{r^{1,(\kappa)}_{j(k)}(\boldsymbol{\tau},\mathbf{p},h,\theta), r^{2,(\kappa)}_{j(k)}(\boldsymbol{\tau},\mathbf{p},h,\theta)\right\},$$

where $r^{(\kappa)}_k(\boldsymbol{\tau},\mathbf{p},h,\theta)$, $r^{1,(\kappa)}_{j(k)}(\boldsymbol{\tau},\mathbf{p},h,\theta)$, and $r^{2,(\kappa)}_{j(k)}(\boldsymbol{\tau},\mathbf{p},h,\theta)$ defined in (19), (27), and (25), respectively.

It remains to deal with the non-convex constraint (1).

*P*roposition 1: From the convexity of the tangential function, it follows that

$$\begin{aligned}&\sqrt{h}\tan\sqrt{\theta}\\ &\geq \sqrt{h}\left(\tan\sqrt{\theta^{(\kappa)}} + \frac{\sqrt{\theta}-\sqrt{\theta^{(\kappa)}}}{(\cos\sqrt{\theta^{(\kappa)}})^2}\right) &(32a)\\ &= \frac{\sin\sqrt{\theta^{(\kappa)}}\cos\sqrt{\theta^{(\kappa)}} - \sqrt{\theta^{(\kappa)}}}{(\cos\sqrt{\theta^{(\kappa)}})^2}\sqrt{h} + \frac{\sqrt{h\theta}}{(\cos\sqrt{\theta^{(\kappa)}})^2} &(32b)\\ &\geq \frac{\sin\sqrt{\theta^{(\kappa)}}\cos\sqrt{\theta^{(\kappa)}} - \sqrt{\theta^{(\kappa)}}}{(\cos\sqrt{\theta^{(\kappa)}})^2}\left(\frac{\sqrt{h^{(\kappa)}}}{2} + \frac{h}{2\sqrt{h^{(\kappa)}}}\right) + \frac{\sqrt{h\theta}}{(\cos\sqrt{\theta^{(\kappa)}})^2}. &(32c)\end{aligned}$$

Proof: See Appendix B.

Therefore, an inner approximation of (1) is[2]

$$R \leq \frac{\sin\sqrt{\theta^{(\kappa)}}\cos\sqrt{\theta^{(\kappa)}} - \sqrt{\theta^{(\kappa)}}}{(\cos\sqrt{\theta^{(\kappa)}})^2}\left(\frac{\sqrt{h^{(\kappa)}}}{2} + \frac{h}{2\sqrt{h^{(\kappa)}}}\right) + \frac{\sqrt{h\theta}}{(\cos\sqrt{\theta^{(\kappa)}})^2}, \quad (33)$$

i.e. every feasible point for the latter is also feasible for the former.

In summary, at the κ-th iteration, we solve the following convex optimization problem to generate the next iterative feasible point $(\tau^{(\kappa+1)}, p^{(\kappa+1)}, \theta^{(\kappa+1)}, h^{(\kappa+1)})$:

$$\max_{\boldsymbol{\tau},\mathbf{p},h,\theta} f^{\text{NOMA},(\kappa)}(\boldsymbol{\tau},\mathbf{p},h,\theta) \quad \text{s.t.} \quad (8b),(8c),(8d),(33). \quad (34)$$

Algorithm 1 outlines the steps to solve the max-min rate optimization problem (8).

Finding an initial feasible point: The initial feasible point $(\boldsymbol{\tau}^{(0)},\mathbf{p}^{(0)},\theta^{(0)},h^{(0)})$ can be obtained by following the following three steps.

1) First, we can calculate $\boldsymbol{\tau}^{(0)}$ and $\mathbf{p}^{(0)}$ by assuming random power and random bandwidth allocation which satisfies (8b) and (8c), i.e.,$\sum_{k=1}^{K/2}\tau^{(0)}_k = 1$ and $\sum_{k=1}^{K} p^{(0)}_k = P$.
2) We can find $\theta^{(0)}$ by fixing it to some value that satisfies $\theta^2_{\min} \leq \theta \leq \theta^2_{\max}$ in (8b).
3) Finally, we can find $h^{(0)}$ by solving a feasibility problem for h under convex constraints $h^2_{\min} \leq h \leq h^2_{max}$ and $R \leq \sqrt{h}\tan\sqrt{\theta^{(0)}}$.

Note that $f^{\text{NOMA},(\kappa)}(\boldsymbol{\tau}^{(\kappa+1)},\mathbf{p}^{(\kappa+1)},h^{(\kappa+1)},\theta^{(\kappa+1)}) > f^{\text{NOMA},(\kappa)}(\boldsymbol{\tau}^{(\kappa)},\mathbf{p}^{(\kappa)},h^{(\kappa)},\theta^{(\kappa)})$ because $(\boldsymbol{\tau}^{(\kappa+1)},\mathbf{p}^{(\kappa+1)},h^{(\kappa+1)},\theta^{(\kappa+1)})$ and $(\boldsymbol{\tau}^{(\kappa)},\mathbf{p}^{(\kappa)},h^{(\kappa)},\theta^{(\kappa)})$ are re-

[2] $\sin\sqrt{\theta^{(\kappa)}}\cos\sqrt{\theta^{(\kappa)}} - \sqrt{\theta^{(\kappa)}} < 0$

Algorithm 1 NOMA-based algorithm for max-min rate optimization problem (8)

Initialization: Set $\kappa := 0$ and a feasible point $(\boldsymbol{\tau}^{(0)}, \mathbf{p}^{(0)}, \theta^{(0)}, h^{(0)})$ for constraints (1), (8b), (8c), and (8d).

1: **repeat**
2: Solve the convex optimization problem (34) to obtain the optimal solution $(\boldsymbol{\tau}^{(\kappa+1)}, \mathbf{p}^{(\kappa+1)}, \theta^{(\kappa+1)}, h^{(\kappa+1)})$.
3: Set $\kappa := \kappa + 1$.
4: **until** Convergence

spectively the optimal solution and a feasible point of (34). Therefore

$$\begin{aligned} & f^{\text{NOMA}}(\boldsymbol{\tau}^{(\kappa+1)}, \mathbf{p}^{(\kappa+1)}, h^{(\kappa+1)}, \theta^{(\kappa+1)}) \\ & \quad \geq f^{\text{NOMA},(\kappa)}(\boldsymbol{\tau}^{(\kappa+1)}, \mathbf{p}^{(\kappa+1)}, h^{(\kappa+1)}, \theta^{(\kappa+1)}) \quad (35) \\ & \quad > f^{\text{NOMA},(\kappa)}(\boldsymbol{\tau}^{(\kappa)}, \mathbf{p}^{(\kappa)}, h^{(\kappa)}, \theta^{(\kappa)}) \\ & \quad = f^{\text{NOMA}}(\boldsymbol{\tau}^{(\kappa)}, \mathbf{p}^{(\kappa)}, h^{(\kappa)}, \theta^{(\kappa)}), \quad (36) \end{aligned}$$

where (35) is true because $f^{\text{NOMA},(\kappa)}$ is a lower bound of f^{NOMA} while (36) is true because $f^{\text{NOMA},(\kappa)}$ matches with f^{NOMA} at $(\boldsymbol{\tau}^{(\kappa)}, \mathbf{p}^{(\kappa)}, h^{(\kappa)}, \theta^{(\kappa)})$, so $(\boldsymbol{\tau}^{(\kappa+1)}, \mathbf{p}^{(\kappa+1)}, h^{(\kappa+1)}, \theta^{(\kappa+1)})$ is a better feasible point than $(\boldsymbol{\tau}^{(\kappa)}, \mathbf{p}^{(\kappa)}, h^{(\kappa)}, \theta^{(\kappa)})$. As such, the sequence $\{(\boldsymbol{\tau}^{(\kappa)}, \mathbf{p}^{(\kappa)}, h^{(\kappa)}, \theta^{(\kappa)})\}$ at least converges to a locally optimal solution of (8) [36], [37].

B. DPC Algorithm

The objective function of the DPC problem (9) is similar to that for the NOMA problem (8). Thus, DPC problem will have the same solution as that of the NOMA problem. Therefore, at the κ-th iteration, we solve the following convex optimization problem to generate the next iterative feasible point $(\tau^{(\kappa+1)}, p^{(\kappa+1)}, \theta^{(\kappa+1)}, h^{(\kappa+1)})$:

$$\begin{aligned} \max_{\boldsymbol{\tau}, \mathbf{p}, h, \theta} \; & f^{\text{DPC},(\kappa)} \triangleq \min_{k=1,\ldots,K/2} \; r_k^{\text{DPC},(\kappa)}(\boldsymbol{\tau}, \mathbf{p}, h, \theta) \\ \text{s.t.} \quad & (8b), (8c), (8d), (33), \end{aligned} \quad (37)$$

where

$$r_k^{\text{DPC},(\kappa)}(\boldsymbol{\tau}, \mathbf{p}, h, \theta) = \begin{cases} r_k^{(\kappa)}(\boldsymbol{\tau}, \mathbf{p}, h, \theta), & k \in \{1, \ldots, K/2\}, \\ r_{j(k)}^{2,(\kappa)}(\boldsymbol{\tau}, \mathbf{p}, h, \theta), & j(k) \in \{K/2+1, \ldots, K\}. \end{cases}$$

Note that $r_k^{(\kappa)}(\boldsymbol{\tau}, \mathbf{p}, h, \theta)$ and $r_{j(k)}^{2,(\kappa)}(\boldsymbol{\tau}, \mathbf{p}, h, \theta)$ are derived in (19) and (25), respectively. Algorithm 2 outlines the steps to solve the max-min rate optimization problem (9).

C. OMA Algorithm

The objective function of the OMA-1 problem (10) also has similarity in its structure to that for the NOMA problem (8). The non-convex constraint (1) can be approximated by (33). Thus, we can use the inequality (13)

Algorithm 2 DPC-based algorithm for max-min rate optimization problem (9)

Initialization: Set $\kappa := 0$ and a feasible point $(\boldsymbol{\tau}^{(0)}, \mathbf{p}^{(0)}, \theta^{(0)}, h^{(0)})$ for constraints (1), (8b), (8c), and (8d).

1: **repeat**
2: Solve the convex optimization problem (37) to obtain the optimal solution $(\boldsymbol{\tau}^{(\kappa+1)}, \mathbf{p}^{(\kappa+1)}, \theta^{(\kappa+1)}, h^{(\kappa+1)})$.
3: Set $\kappa := \kappa + 1$.
4: **until** Convergence

Algorithm 3 OMA-1 algorithm for max-min rate optimization problem (10)

Initialization: Set $\kappa := 0$ and a feasible point $(\boldsymbol{\tau}^{(0)}, \mathbf{p}^{(0)}, \theta^{(0)}, h^{(0)})$ for constraints (1), (8b), (10b), and (8d).

1: **repeat**
2: Solve the convex optimization problem (38) to obtain the optimal solution $(\boldsymbol{\tau}^{(\kappa+1)}, \mathbf{p}^{(\kappa+1)}, \theta^{(\kappa+1)}, h^{(\kappa+1)})$.
3: Set $\kappa := \kappa + 1$.
4: **until** Convergence

and the approximations (16) and (17) to approximate the non-concave objective function in (10). Thus, we solve the following convex optimization problem, at the κ-th iteration, to generate the next iterative feasible point $(\tau^{(\kappa+1)}, p^{(\kappa+1)}, \theta^{(\kappa+1)}, h^{(\kappa+1)})$:

$$\begin{aligned} \max_{\boldsymbol{\tau}, \mathbf{p}, h, \theta} \; & f^{\text{OMA-1},(\kappa)} \triangleq \min_{k=1,\ldots,K} \; r_k^{\text{OMA-1},(\kappa)}(\boldsymbol{\tau}, \mathbf{p}, h, \theta) \\ \text{s.t.} \quad & (8b), (10b), (8d), (33), \end{aligned} \quad (38)$$

where $r_k^{\text{OMA-1},(\kappa)}(\boldsymbol{\tau}, \mathbf{p}, h, \theta) = r_k^{(\kappa)}(\boldsymbol{\tau}, \mathbf{p}, h, \theta), \; \forall \; k = \{1, \ldots, K\}$ and $r_k^{(\kappa)}(\boldsymbol{\tau}, \mathbf{p}, h, \theta)$ is defined in (19). Algorithm 3 outlines the steps to solve the max-min rate optimization problem (10). The initial feasible point $(\boldsymbol{\tau}^{(0)}, \mathbf{p}^{(0)}, \theta^{(0)}, h^{(0)})$ can be obtained in the same way as described for the NOMA in Section III-A.

Next, in order to solve the OMA-2 problem (11), at the κ-th iteration, we solve the following convex optimization problem to generate the next iterative feasible point $(\tau^{(\kappa+1)}, p^{(\kappa+1)}, \theta^{(\kappa+1)}, h^{(\kappa+1)})$:

$$\begin{aligned} \max_{\boldsymbol{\tau}, \mathbf{p}, h, \theta} \; & f^{\text{OMA-2},(\kappa)} \min_{k=1,\ldots,K/2} \; r_k^{\text{OMA-2},(\kappa)}(\boldsymbol{\tau}, \mathbf{p}, h, \theta) \\ \text{s.t.} \quad & (8b), (8c), (8d), (33), \end{aligned} \quad (39)$$

where

$$r_k^{\text{OMA-2},(\kappa)}(\boldsymbol{\tau}, \mathbf{p}, h, \theta) = \begin{cases} r_k^{\text{O},(\kappa)}(\boldsymbol{\tau}, \mathbf{p}, h, \theta), & k \in \{1, \ldots, K/2\}, \\ r_{j(k)}^{\text{O},(\kappa)}(\boldsymbol{\tau}, \mathbf{p}, h, \theta), & j(k) \in \{K/2+1, \ldots, K\}, \end{cases}$$

where $r_k^{\text{O},(\kappa)}(\boldsymbol{\tau}, \mathbf{p}, h, \theta)$ and $r_{j(k)}^{\text{O},(\kappa)}(\boldsymbol{\tau}, \mathbf{p}, h, \theta)$ are inner approximations (at the κ-th iteration) of the non-concave

functions $r_k^{\mathrm{O}}(\boldsymbol{\tau},\mathbf{p},h,\theta)$ and $r_{j(k)}^{\mathrm{O}}(\boldsymbol{\tau},\mathbf{p},h,\theta)$, respectively (defined in (12)). Since $r_{j(k)}^{\mathrm{O}}(\boldsymbol{\tau},\mathbf{p},h,\theta)$ is similar to the rate function $r_{j(k)}^{2}(\boldsymbol{\tau},\mathbf{p},h,\theta)$ (defined in (6) for the NOMA-problem) and $r_k^{\mathrm{O}}(\boldsymbol{\tau},\mathbf{p},h,\theta)$ has similar structure too, we can use the inequality (13) (given in Lemma 1) and the approximations (22) and (23) to find the inner approximations $r_k^{\mathrm{O},(\kappa)}(\boldsymbol{\tau},\mathbf{p},h,\theta)$ and $r_{j(k)}^{\mathrm{O},(\kappa)}(\boldsymbol{\tau},\mathbf{p},h,\theta)$.

Thus, by applying the inequality (13) for

$$\tau=\tau_k\ \ ,\quad x=\sigma_B\theta/g_o\tilde{g}_k p_k,$$
$$y=\tau_k(d_k+h)^{\alpha/2}+g_o\tilde{g}_k p_{j(k)}/(\sigma_B\theta),$$

we can obtain the inner approximation for the non-concave rate function $r_k^{\mathrm{O}}(\boldsymbol{\tau},\mathbf{p},h,\theta)$, as follows:

$$r_k^{\mathrm{O},(\kappa)}(\boldsymbol{\tau},\mathbf{p},h,\theta)\triangleq\tilde{a}_k^{O,(\kappa)}+\tilde{b}_k^{O,(\kappa)}\Big(2-\pi_k^{(\kappa)}(\theta,p_k)-\tilde{\nu}_{j(k)}^{O,(\kappa)}(\tau_k,p_{j(k)},\theta)\Big)-\frac{\tilde{c}_k^{O,(\kappa)}}{\tau_k},\tag{40}$$

where

$$\tilde{\nu}_{j(k)}^{O,(\kappa)}(\tau_k,p_{j(k)},\theta)\triangleq\frac{1}{4}\frac{\Big((\tau_k/\tau_k^{(\kappa)})+(d_k+h)^{\alpha/2}/(d_k+h^{(\kappa)})^{\alpha/2}\Big)^2}{1+g_o\tilde{g}_k p_{j(k)}^{(\kappa)}/\sigma_B\theta^{(\kappa)}\tau_k^{(\kappa)}(d_k+h^{(\kappa)})^{\alpha/2}}+\frac{1}{4}\frac{\Big((p_{j(k)}/p_{j(k)}^{(\kappa)})+(\theta^{(\kappa)}/\theta)\Big)^2}{\sigma_B\theta^{(\kappa)}\tau_k^{(\kappa)}(d_k+h^{(\kappa)})^{\alpha/2}/g_o\tilde{g}_k p_{j(k)}^{(\kappa)}+1},\tag{41}$$

and

$$\tilde{a}_k^{O,(\kappa)}=2\bar{\tau}\ln(1+1/\bar{x}\bar{y}),$$
$$\tilde{b}_k^{O,(\kappa)}=\frac{\bar{\tau}}{1+\bar{x}\bar{y}},$$
$$\tilde{c}_k^{O,(\kappa)}=\bar{\tau}^2\ln(1+1/\bar{x}\bar{y}),\tag{42}$$

under

$$\bar{\tau}=\tau_k^{(\kappa)}\ \ ,\quad \bar{x}=\sigma_B\theta^{(\kappa)}/g_o\tilde{g}_k p_k^{(\kappa)},$$
$$\bar{y}=\tau_k^{(\kappa)}(d_k+h^{(\kappa)})^{\alpha/2}+g_o\tilde{g}_k p_{j(k)}^{(\kappa)}/(\sigma_B\theta^{(\kappa)}).$$

Similarly, by applying the inequality (13) for

$$\tau=\tau_k, x=\sigma_B\theta/g_o\tilde{g}_{j(k)}p_{j(k)},$$
$$y=\tau_k(d_{j(k)}+h)^{\alpha/2}+g_o\tilde{g}_{j(k)}p_k/(\sigma_B\theta),$$

we can obtain the inner approximation for the non-concave rate function $r_{j(k)}^{\mathrm{O}}(\boldsymbol{\tau},\mathbf{p},h,\theta)$ as follows:

$$r_{j(k)}^{O,(\kappa)}(\boldsymbol{\tau},\mathbf{p},h,\theta)\triangleq\tilde{a}_{j(k)}^{O,(\kappa)}+\tilde{b}_{j(k)}^{O,(\kappa)}\Big(2-\pi_{j(k)}^{(\kappa)}(\theta,p_{j(k)})-\tilde{\nu}_k^{O,(\kappa)}(\tau_k,p_k,\theta)\Big)-\frac{\tilde{c}_{j(k)}^{O,(\kappa)}}{\tau_k},\tag{43}$$

Algorithm 4 OMA-2 algorithm for max-min rate optimization problem (11)

Initialization: Set $\kappa:=0$ and a feasible point $(\boldsymbol{\tau}^{(0)},\mathbf{p}^{(0)},\theta^{(0)},h^{(0)})$ for constraints (1), (8b), (8c), and (8d).

1: **repeat**
2: Solve the convex optimization problem (39) to obtain the optimal solution $(\boldsymbol{\tau}^{(\kappa+1)},\mathbf{p}^{(\kappa+1)},\theta^{(\kappa+1)},h^{(\kappa+1)})$.
3: Set $\kappa:=\kappa+1$.
4: **until** Convergence

where

$$\tilde{\nu}_k^{O,(\kappa)}(\tau_k,p_k,\theta)\triangleq\frac{1}{4}\frac{\Big((\tau_k/\tau_k^{(\kappa)})+(d_{j(k)}+h)^{\alpha/2}/(d_{j(k)}+h^{(\kappa)})^{\alpha/2}\Big)^2}{1+g_o\tilde{g}_{j(k)}p_k^{(\kappa)}/\sigma_B\theta^{(\kappa)}\tau_k^{(\kappa)}(d_{j(k)}+h^{(\kappa)})^{\alpha/2}}+\frac{1}{4}\frac{\Big((p_k/p_k^{(\kappa)})+(\theta^{(\kappa)}/\theta)\Big)^2}{\sigma_B\theta^{(\kappa)}\tau_k^{(\kappa)}(d_{j(k)}+h^{(\kappa)})^{\alpha/2}/g_o\tilde{g}_{j(k)}p_k^{(\kappa)}+1},\tag{44}$$

and

$$\tilde{a}_{j(k)}^{O,(\kappa)}=2\bar{\tau}\ln(1+1/\bar{x}\bar{y}),$$
$$\tilde{b}_{j(k)}^{O,(\kappa)}=\frac{\bar{\tau}}{1+\bar{x}\bar{y}},$$
$$\tilde{c}_{j(k)}^{O,(\kappa)}=\bar{\tau}^2\ln(1+1/\bar{x}\bar{y}),\tag{45}$$

under

$$\bar{\tau}=\tau_k^{(\kappa)}//,///\bar{x}=\sigma_B\theta^{(\kappa)}/g_o\tilde{g}_{j(k)}p_{j(k)}^{(\kappa)},$$
$$\bar{y}=\tau_k^{(\kappa)}(d_{j(k)}+h^{(\kappa)})^{\alpha/2}+g_o\tilde{g}_{j(k)}p_k^{(\kappa)}/(\sigma_B\theta^{(\kappa)}).$$

Algorithm 4 outlines the steps to solve the max-min rate optimization problem (11). The initial feasible point $(\boldsymbol{\tau}^{(0)},\mathbf{p}^{(0)},\theta^{(0)},h^{(0)})$ can be obtained in the same way as described for the NOMA in Section III-A.

Before closing this section, let us mention that it is possible to extend our computational approach to scenarios of multiple UAVs serving their own users and thus creating multiple cells as follows. For simplicity of explanation, suppose that each UAV serves the same number K of ground users so the total bandwidth is divided and re-used in each cell for spectral efficiency. To cancel inter-cell interference, which is difficult to be enhanced due to the poor scattering of the air-to-ground (A2G) channels, one simply allocates different bandwidths to users on cell boundary, i.e. those on cell boundary from different cells are allocated different bandwidths. As such (8) (for NOMA), (9) (for DPC), (10) (for OMA-1) and (11) (for OMA-1) will involve the same variable $\boldsymbol{\tau}$ of bandwidth allocation satisfying the constraint (8c) or (10b) but each cell i has its own variables $\mathbf{p}^{(i)}$, $h^{(i)}$, and $\theta^{(i)}$ of power allocation for its

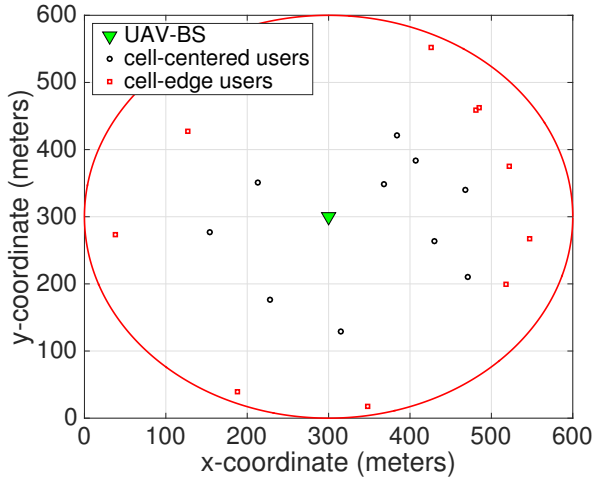

Fig. 2. Network topology used in the simulations.

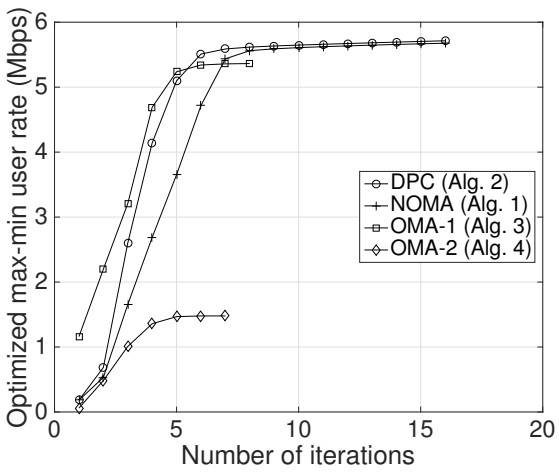

Fig. 3. The convergence of the proposed Algorithms 1-4.

users, UAV's altitude and beamwidth, which are independently constrained. Thus, all the proposed algorithms can be adjusted for computational solution of these problems.

IV. Simulation Results

In this section, we analyze the performance of the proposed Algorithms 1-4 via simulations. We use the network topology as used in Fig. 2, where the cell radius is set to $R = 300$ meters, and there are $K = 20$ users randomly placed within the cell. The UAV BS is at the cell-center and at altitude $\sqrt{h}$ above the ground-level. Fig. 2 shows the ground-level projection of the UAV BS. Half of the users are placed closer to the UAV BS, while the rest of the users are farther from the UAV BS. The channel power gain g_o at a distance of 1 meter is set to 3.24×10^{-4}, which incorporates -38.47 dB (1.42×10^{-4}) path loss and antenna gain 2.2846 [18]. The Rician factor for the Rician fading channel $\tilde{h}_k$ is set to $K_R = 12$ dB [31]. The maximum and minimum UAV altitude are set to $h_{\max} = 500$ meters and $h_{\min} = 50$ meters, respectively. The range of the antenna beamwidth is set to $\theta_{\min} = 0$ and $\theta_{\max} = \pi/2$ rad. The total power budget is $P = 2$ mW (3 dBm). Unless stated otherwise, we set total available bandwidth $\mathcal{B} = 15$ MHz, the noise power density $\sigma^2 = -174$ dBm/Hz, and the path-loss exponent $\alpha = 2$ [9], [20]. However, in this section, we will also test our proposed algorithms for different values of $\mathcal{B}$, σ^2, and α. The simulations are run by using MATLAB and off-the-shelf solvers such as CVX [38].

A. Performance of the Proposed Algorithms 1-4

Fig. 3 plots the convergence results of the proposed Algorithms 1-4 employing NOMA problem (8), DPC problem (9), OMA-1 problem (10), and OMA-2 problem (11), respectively. Fig. 3 shows that NOMA (Alg. 1) and DPC (Alg. 2) take around 16 iterations to converge. On the other hand, the convergence of the OMA-1 and OMA-2 (Algorithms 3 and 4) requires only eight and seven iterations, respectively. However, the NOMA and DPC achieve better rates than their OMA counterparts. Even, at the sventh iteration, which is the point where the OMA-1 (Alg. 3) converges, the optimized rates of the NOMA and DPC are better than that of the OMA-1.

The computational complexity of NOMA (Alg. 1) is $\mathcal{O}\left(i_{\text{A1}}(1.5K+2)^3(2K+7)\right)$, DPC (Alg. 2) is $\mathcal{O}\left(i_{\text{A2}}(1.5K+2)^3(2K+7)\right)$, OMA-1 (Alg. 3) is $\mathcal{O}\left(i_{\text{A3}}(2K+2)^3(2K+7)\right)$, and OMA-2 (Alg. 4) is $\mathcal{O}\left(i_{\text{A4}}(1.5K+2)^3(2K+7)\right)$ [39, p. 4], where $i_{\text{A1}} = 16$, $i_{\text{A2}} = 17.2$, $i_{\text{A3}} = 7$, $i_{\text{A4}} = 6$ are the average number of iterations required for the convergence of Algorithms 1, 2, 3, and 4, respectively.

Fig. 4 plots the optimized max-min user rate versus the total available bandwidth $\mathcal{B}$. We solve NOMA problem (8), DPC problem (9), OMA-1 problem (10), and OMA-2 problem (11) using Algorithms 1, 2, 3, and 4, respectively. As expected, the optimized rate increases with an increase in the total available bandwidth $\mathcal{B}$. Fig. 4 shows that the performance of NOMA is quite closer to that of the DPC while clearly better than that of the OMA counterparts. Moreover, we observe that the performance gap between the NOMA and OMA-1 increases with an increase in the available bandwidth $\mathcal{B}$.

Fig. 5 plots the optimized max-min user rates of the proposed Algorithms 1-4 versus the noise power density σ^2. As expected, the optimized rate decreases with an increase in the noise power density σ^2. Fig. 5 again shows the same trend that the NOMA and DPC clearly outperform the OMA counterparts. In addition, the performance gap between the NOMA and OMA-1 decreases as the noise power density σ^2 increases.

Figs. 6 and 7 plot the optimized values of UAV altitude and antenna beamwidth, respectively, after solving all the

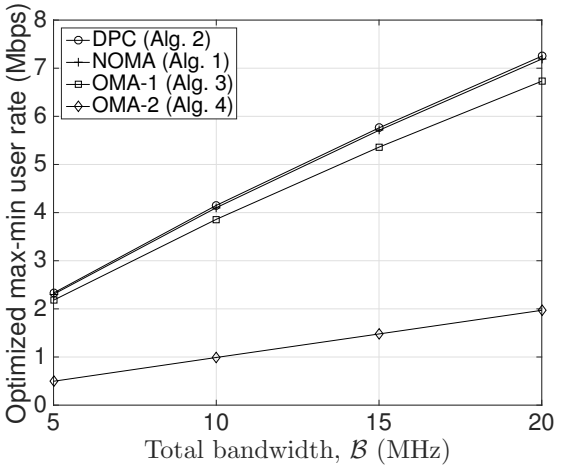

Fig. 4. Optimized max-min user rate versus total available bandwidth $\mathcal{B}$, for the noise power density $\sigma^2 = -174$ dBm/Hz.

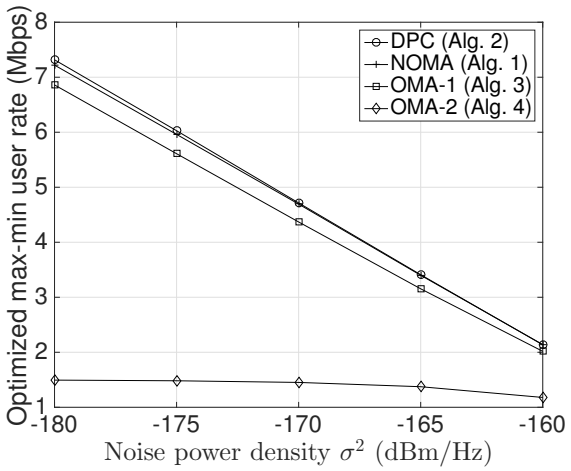

Fig. 5. Optimized max-min user rate versus noise power density σ^2, where the available bandwidth is set to $\mathcal{B} = 15$ MHz.

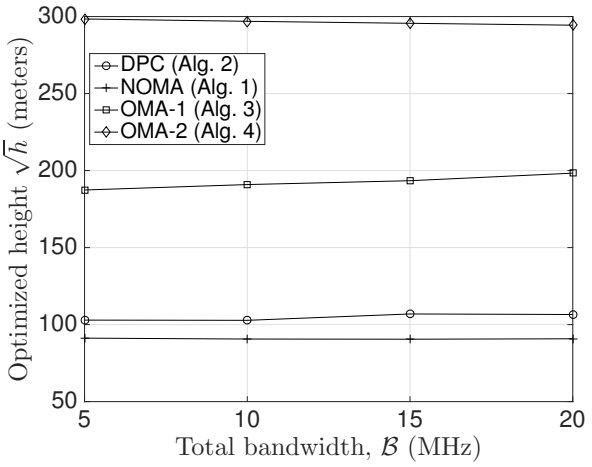

Fig. 6. Optimized altitude $\sqrt{h}$ versus total available bandwidth $\mathcal{B}$, where the noise power density is set to $\sigma^2 = -174$ dBm/Hz.

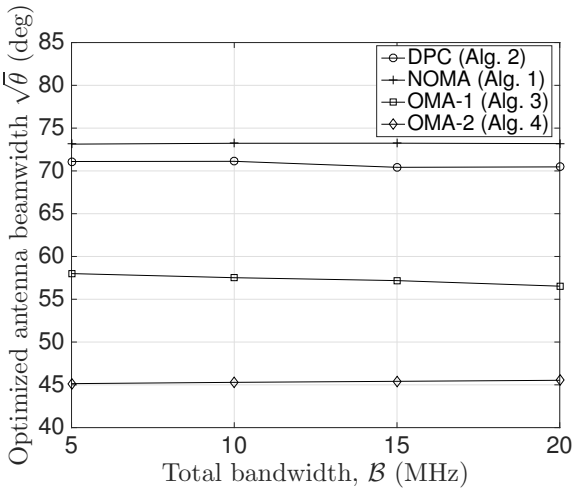

Fig. 7. Optimized antenna beamwidth $\sqrt{\theta}$ versus total available bandwidth $\mathcal{B}$, where the noise power density is set to $\sigma^2 = -174$ dBm/Hz.

problems using Algorithms 1, 2, 3, and 4. Figs. 6 and 7 show that there is minor change in the optimized values of the UAV altitude and antenna beamwidth for different values of the total available bandwidth $\mathcal{B}$. This is an interesting and desirable result since the UAV is not required to move much if the bandwidth quota changes.

Fig. 8 plots the optimized max-min rates of the proposed Algorithms 1-4 versus the path-loss exponent, α. This results has been simulated since some recent studies [30], [31] adopt higher values of path-loss exponent for UAV communication. Fig. 5 shows an interesting and promising result that for higher values of path-loss exponent, the performance gap between the NOMA and DPC vanishes, while they clearly outperform the OMA counterparts. On the other hand, as expected, the optimized rate for all the algorithms decreases with an increase in α.

B. Comparison with the Sub-optimal Schemes

Fig. 9 plots the optimized max-min user rate for sub-optimal strategy where only power and bandwidth are optimized under fixed altitude $\sqrt{h}$ and fixed antenna beamwidth $\sqrt{\theta}$, such that the constraint (1) is satisfied. Again, the bandwidth is set to $\mathcal{B} = 15$ MHz. Fig. 9(a) assumes $\sqrt{h} = 100$ m while Fig. 9(b) assumes $\sqrt{h} = 200$ m. That is, in Fig. 9, we solve the NOMA problem (8), the DPC problem (9), and the OMA-1 problem (10), for given fixed altitude $\sqrt{h}$ and fixed antenna beamwidth $\sqrt{\theta}$, i.e., in the absence of constraint (1). Thus, this sub-optimal scheme requires solving only for the optimal power $\mathbf{p}$ and optimal bandwidth allocation $\boldsymbol{\tau}$. The optimized max-min rates are clearly smaller than the optimized rates as obtained by the proposed optimal Algorithms 1-3, which are shown by the black bar at the left of each group in Fig. 9. This is because Algorithms 1-4 jointly optimize all

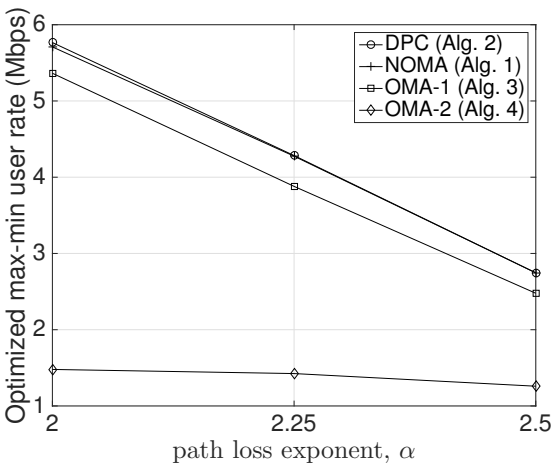

Fig. 8. Optimized max-min user rate versus the path-loss exponent, α.

the parameters. In addition, *this justifies the desirability of optimizing UAV-BS altitude and antenna beamwidth*. Note that the Fig. 9 does not plot results for OMA-2 (Alg. 4) because it performs quite poorly than the other three algorithms.

Fig. 10 plots the max-min user rate obtained by another sub-optimal scheme, which assumes fixed power $\mathbf{p}$ and fixed bandwidth $\boldsymbol{\tau}$ allocation and solves to find the optimal UAV altitude $\sqrt{h}$ and optimal antenna beamwidth $\sqrt{\theta}$. Particularly, we opt for equal power and equal bandwidth allocation, such that, equal power allocation implies $p_k = P/K$, $\forall\ k$, while equal bandwidth for the NOMA and DPC mean $\tau_k = 1/(K/2)$, $\forall\ k \in \{1, \ldots, K/2\}$ and equal bandwidth allocation for OMA-1 means $\tau_k = 1/K$, $\forall\ k \in \{1, \ldots, K\}$. Fig. 10 shows that optimal schemes (Algorithms 1, 2, and 3 plotted with solid lines) clearly outperform the respective sub-optimal schemes (plotted with dashed lines). Fig. 10 shows that the sub-optimal NOMA and the sub-optimal DPC perform quite poorly, and even deliver a worse rate than the sub-optimal OMA-1. This is because wise power allocation is necessary for the NOMA and DPC, whereas, the sub-optimal NOMA and the sub-optimal DPC in Fig. 10 assume equal power allocation, which worsen their achievable rate.

V. Conclusions

In this paper, we have considered a UAV-enabled communication network which serves a large number of users by employing NOMA. We have formulated the max-min rate optimization problem under total power, total bandwidth, UAV altitude, and antenna beamwidth constraints. The formulated max-min rate objective function is non-convex in the optimization variables, i.e., the UAV's flying altitude, transmit antenna beamwidth, power allocation and bandwidth allocation for multiple users. We have developed a path-following algorithm to solve the formulated problem. In addition, we have also formulated OMA and DPC-based max-min rate optimization problems and developed respective path-following algorithms to solve them. Finally, our numerical results show that NOMA outperforms OMA and achieves rates similar to those achieved by DPC. Moreover, we have observed a clear rate gain by jointly optimizing all the parameters (power, bandwidth, UAV altitude, and antennas beamwidth), when compared to the case of optimizing subset of these parameters, which confirms the desirability of their joint optimization. Physical layer security for UAV-enabled communication is an very important issue and is under our study.

Appendix A
Proof of Lemma 1

For the convex function $f(x, y, t) \triangleq \ln(1 + 1/xy)^{1/t}$ [40], one has the following inequality for every $x > 0$, $y > 0$, $t > 0$, $\bar{x} > 0$, $\bar{y} > 0$ and $\bar{t} > 0$:

$$\begin{aligned}\frac{\ln(1+1/xy)}{t} &= f(x,y,t)\\ &\geq f(\bar{x},\bar{y},\bar{t}) + \langle \nabla f(\bar{x},\bar{y},\bar{t}), (x,y,t) - (\bar{x},\bar{y},\bar{t})\rangle\\ &= \frac{2\ln(1+1/\bar{x}\bar{y})}{\bar{t}} + \frac{1}{\bar{t}(1+\bar{x}\bar{y})}(2 - x/\bar{x} - y/\bar{y})\\ &\quad - \frac{\ln(1+1/\bar{x}\bar{y})}{\bar{t}^2}t \quad (46)\end{aligned}$$

Therefore, by setting $\tau = 1/t$ and $\bar{\tau} = 1/\bar{t}$, we can achieve the following inequality.

$$\tau \ln\left(1 + \frac{1}{xy}\right) \geq 2\bar{\tau}\ln\left(1 + \frac{1}{\bar{x}\bar{y}}\right) + \frac{\bar{\tau}\,(2 - x/\bar{x} - y/\bar{y})}{1 + \bar{x}\bar{y}} - \frac{\bar{\tau}^2 \ln(1 + 1/\bar{x}\bar{y})}{\tau}$$

Appendix B
Proof of Proposition 1

The convex function $f(x)$ can be approximated by the following lower bound at $x = x^{(\kappa)}$,

$$f(x) \geq f(x^{(\kappa)}) + \nabla_x f(x^{(\kappa)})(x - x^{(\kappa)}) \quad (47)$$

and concave function $g(x)$ can be approximated by the following upper bound at $x = x^{(\kappa)}$,

$$g(x) \leq g(x^{(\kappa)}) + \nabla_x g(x^{(\kappa)})(x - x^{(\kappa)}) \quad (48)$$

where $\nabla_x f(x^{(\kappa)})$ is the gradient of function $f(x)$ with respect to its variable x and evaluated at $x = x^{(\kappa)}$.

Using (47), the convex tangent function can be approximated by

$$\tan\sqrt{\theta} \geq \tan\sqrt{\theta^{(\kappa)}} + \frac{\sqrt{\theta} - \sqrt{\theta^{(\kappa)}}}{(\cos\sqrt{\theta^{(\kappa)}})^2} \quad (49)$$

From (49), we can achieve (32a) or equivalently (32b) in Proposition 1.

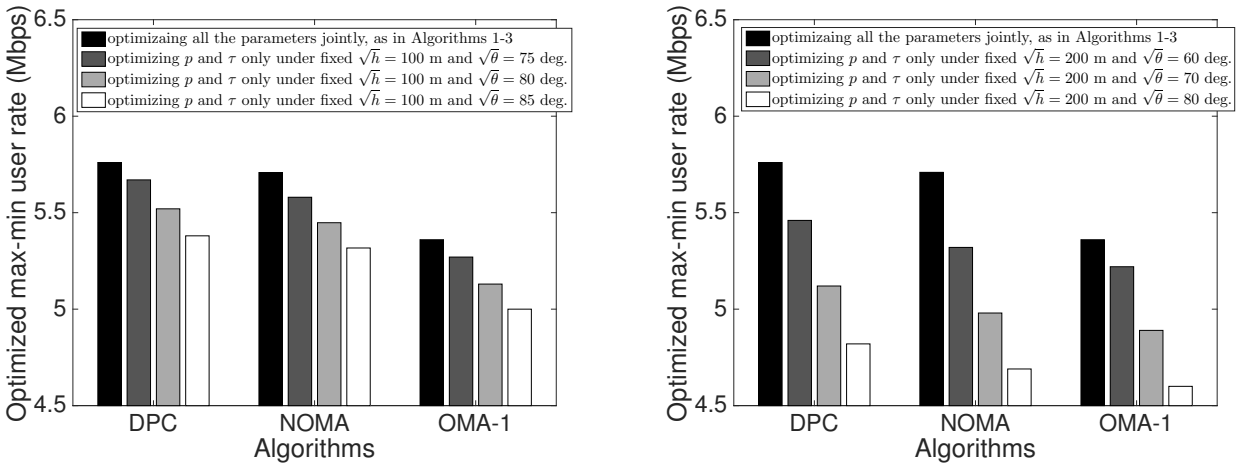

(a) (b)

Fig. 9. Comparison of max-min user rate obtained by optimizing only power and bandwidth under fixed altitude $\sqrt{h}$ and fixed antenna beamwidth $\sqrt{\theta}$ (satisfying (1)) with the max-min rate achieved by optimizing all the parameters jointly by proposed Algorithms (shown by black bar at the left of each group). Subfig. (a) assumes $\sqrt{h}=100$ m and subfig. (b) assumes $\sqrt{h}=200$ m.

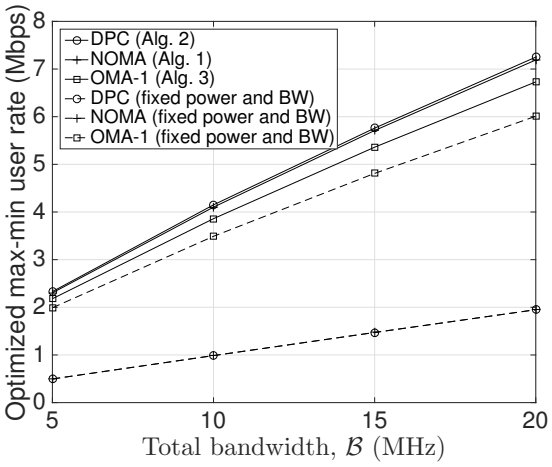

Fig. 10. Comparison of the optimized max-min user rate obtained under fixed power $\mathbf{p}$ and fixed bandwidth $\boldsymbol{\tau}$ allocation (equal power and equal bandwidth allocation) with the optimized max-min rate achieved by the proposed algorithms.

Next, using (48), the concave function $\sqrt{h}$ can be approximated by

$$\sqrt{h} \leq \frac{\sqrt{h^{(\kappa)}}}{2} + \frac{h}{2\sqrt{h^{(\kappa)}}} \tag{50}$$

Using (50) in (32b), we can achieve the final expression (32c) in Proposition 1.

REFERENCES

[1] Y. Zeng, R. Zhang, and T. J. Lim, "Throughput maximization for UAV-enabled mobile relaying systems," *IEEE Trans. Commun.*, vol. 64, no. 12, pp. 4983–4996, Dec. 2016.

[2] F. Jiang and A. L. Swindlehurst, "Optimization of UAV heading for the ground-to-air uplink," *J. Sel. Areas Commun.*, vol. 30, no. 5, pp. 993–1005, June 2012.

[3] I. Bor-Yaliniz and H. Yanikomeroglu, "The new frontier in RAN heterogeneity: Multi-tier drone-cells," *IEEE Commun. Mag.*, vol. 54, no. 11, pp. 48–55, Nov. 2016.

[4] H. Menouar, I. Guvenc, K. Akkaya, A. S. Uluagac, A. Kadri, and A. Tuncer, "UAV-enabled intelligent transportation systems for the smart city: Applications and challenges," *IEEE Commun. Mag.*, vol. 55, no. 3, pp. 22–28, Mar. 2017.

[5] M. Mozaffari, W. Saad, M. Bennis, and M. Debbah, "Mobile unmanned aerial vehicles (UAVs) for energy-efficient internet of things communications," *IEEE Trans. Wirel. Commun.*, vol. 16, no. 11, pp. 7574–7589, Nov. 2017.

[6] GSMA. Mobile-enabled unmanned aircraft. [Online]. Available: https://www.gsma.com/iot/mobile-enabled-unmanned-aircraft/

[7] P. Zhan, K. Yu, and A. L. Swindlehurst, "Wireless relay communications with unmanned aerial vehicles: Performance and optimization," *IEEE Trans. Aerosp. Electron. Syst.*, vol. 47, no. 3, pp. 2068–2085, 2011.

[8] M. Erdelj, E. Natalizio, K. R. Chowdhury, and I. F. Akyildiz, "Help from the sky: Leveraging UAVs for disaster management," *IEEE Pervasive Comput.*, vol. 16, no. 1, pp. 24–32, Jan. 2017.

[9] F. Ono, H. Ochiai, and R. Miura, "A wireless relay network based on unmanned aircraft system with rate optimization," *IEEE Trans. Wirel. Commun.*, vol. 15, no. 11, pp. 7699–7708, Nov. 2016.

[10] A. Merwaday, A. Tuncer, A. Kumbhar, and I. Guvenc, "Improved throughput coverage in natural disasters: Unmanned aerial base stations for public-safety communications," *IEEE Veh. Technol. Mag.*, vol. 11, no. 4, pp. 53–60, Dec. 2016.

[11] Y. Zeng, R. Zhang, and T. J. Lim, "Wireless communications with unmanned aerial vehicles: opportunities and challenges," *IEEE Commun. Mag.*, vol. 54, no. 5, pp. 36–42, May 2016.

[12] Y. Zeng and R. Zhang, "Energy-efficient UAV communication with trajectory optimization," *IEEE Trans. Wirel. Commun.*, vol. 16, no. 6, pp. 3747–3760, Jun. 2017.

[13] V. V. Chetlur and H. S. Dhillon, "Downlink coverage analysis for a finite 3-D wireless network of unmanned aerial vehicles," *IEEE Trans. Commun.*, vol. 65, no. 10, pp. 4543–4558, Oct. 2017.

[14] Y. Zeng, X. Xu, and R. Zhang, "Trajectory design for completion time minimization in UAV-enabled multicasting," *IEEE Trans. Wirel. Commun.*, vol. 17, no. 4, pp. 2233–2246, Apr. 2018.

[15] Q. Wu, L. Liu, and R. Zhang, "Fundamental tradeoffs in communication and trajectory design for UAV-enabled wireless network," *ArXiv Technical Report*, 2018. [Online]. Available: https://arxiv.org/abs/1805.07038

[16] Y. Zhou, N. Cheng, N. Lu, and X. S. Shen, "Multi-UAV-aided networks: Aerial-ground cooperative vehicular networking architecture," *IEEE Veh. Technol. Mag.*, vol. 10, no. 4, pp. 36–44, Dec 2015.

[17] Q. Wu, Y. Zeng, and R. Zhang, "Joint trajectory and communication design for multi-UAV enabled wireless networks," *IEEE Trans. Wireless Commun.*, vol. 17, no. 3, pp. 2109–2121, March 2018.
[18] H. He, S. Zhang, Y. Zeng, and R. Zhang, "Joint altitude and beamwidth optimization for UAV-enabled multiuser communications," *IEEE Commun. Lett.*, vol. 22, no. 2, pp. 344–347, 2018.
[19] H. Wang, J. Wang, G. Ding, L. Wang, T. A. Tsiftsis, and P. K. Sharma, "Resource allocation for energy harvesting-powered D2D communication underlaying UAV-assisted networks," *IEEE Trans. Green Commun. Netw.*, vol. 2, no. 1, pp. 14–24, Mar. 2018.
[20] H. Ghazzai, M. B. Ghorbel, A. Kadri, M. J. Hossain, and H. Menouar, "Energy-efficient management of unmanned aerial vehicles for underlay cognitive radio systems," *IEEE Trans. Green Commun. Netw.*, vol. 1, no. 4, pp. 434–443, Dec. 2017.
[21] J. Lyu, Y. Zeng, and R. Zhang, "UAV-Aided offloading for cellular hotspot," *IEEE Trans. Wirel. Commun.*, vol. 17, no. 6, pp. 3988–4001, 2018.
[22] Q. Wu and R. Zhang, "Common throughput maximization in UAV-enabled OFDMA systems with delay consideration," *IEEE Trans. Commun.*, vol. 12, no. 66, pp. 6614–6627, Dec. 2018.
[23] Y. Saito, Y. Kishiyama, A. Benjebbour, T. Nakamura, A. Li, and K. Higuchi, "Non-orthogonal multiple access (NOMA) for cellular future radio access," in *Proc. IEEE Veh. Technol. Conf. (VTC Spring)*, June 2013, pp. 1–5.
[24] Z. Ding et al., "Application of non-orthogonal multiple access in LTE and 5G networks," *IEEE Commun. Mag.*, vol. 55, no. 2, pp. 185–191, Feb. 2017.
[25] Z. Ding, F. Adachi, and H. V. Poor, "The application of MIMO to non-orthogonal multiple access," *IEEE Trans. Wireless Commun.*, vol. 15, no. 1, pp. 537–552, Jan. 1016.
[26] V. D. Nguyen, H. D. Tuan, T. Q. Duong, H. V. Poor, and O. S. Shin, "Precoder design for signal superposition in MIMO-NOMA multicell networks," *IEEE J. Selec. Areas Commun.*, vol. 35, no. 12, pp. 2681–2695, Dec. 2017.
[27] P. K. Sharma and D. I. Kim, "UAV-enabled downlink wireless system with non-orthogonal multiple access," in *Proc. IEEE Global Commun. Conf.*, Dec. 2017, pp. 1–6.
[28] Q. Wu, J. Xu, and R. Zhang, "Capacity characterization of UAV-enabled two-user broadcast channel," *IEEE J. Selec. Areas Communs.*, vol. 36, no. 9, pp. 1955–1971, Sep. 2018.
[29] N. Rupasinghe, Y. Yapici, I. Guvenc, and Y. Kakishima, "Non-orthogonal multiple access for mmwave drones with multi-antenna transmission," *https://arxiv.org/pdf/1711.10050.pdf*, 2018.
[30] M. F. Sohail, C. Y. Leow, and S. H. Won, "Non-orthogonal multiple access for unmanned aerial vehicle assisted communication," *IEEE Access*, vol. 6, pp. 22 716 – 22 727, Apr. 2018.
[31] M. M. Azari, F. Rosas, K.-C. Chen, and S. Pollin, "Ultra reliable UAV communication using altitude and cooperation diversity," *IEEE Trans. Commun.*, vol. 66, no. 1, pp. 330–344, Jan. 2018.
[32] Z. Ding, P. Fan, and H. V. Poor, "Impact of user pairing on 5G nonorthogonal multiple-access downlink transmissions," *IEEE Trans. Veh. Technol.*, vol. 65, no. 8, pp. 6010–6023, Aug. 2016.
[33] W. Yu and J. M. Cioffi, "Trellis precoding for the broadcast channel," in *Proc. IEEE Global Commun. Conf.*, Nov. 2001, pp. 1344–1383.
[34] U. Erez and S. ten Brink, "A close-to-capacity dirty paper coding scheme," *IEEE Trans. Inf. Theory*, vol. 51, no. 10, pp. 3417–3432, Oct. 2005.
[35] U. Erez, S. Shamai, and R. Zamir, "Capacity and lattice strategies for canceling known interference," *IEEE Trans. Inf. Theory*, vol. 51, no. 11, pp. 3820–3833, Nov. 2005.
[36] H. H. M. Tam, H. D. Tuan, and D. T. Ngo, "Successive convex quadratic programming for quality-of-service management in full-duplex MU-MIMO multicell networks," *IEEE Trans. Commun.*, vol. 64, no. 6, pp. 2340–2353, Jun. 2016.
[37] H. H. M. Tam, H. D. Tuan, D. T. Ngo, T. Q. Duong, and H. V. Poor, "Joint load balancing and interference management for small-cell heterogeneous networks with limited backhaul capacity," *IEEE Trans. Wirel. Commun.*, vol. 16, no. 2, pp. 872–884, Feb. 2017.
[38] M. Grant and S. Boyd, "CVX: Matlab software for disciplined convex programming, version 2.1," http://cvxr.com/cvx, Mar. 2014.
[39] D. Peaucelle, D. Henrion, and Y. Labit, "Users guide for SeDuMi interface 1.03," 2002. [Online]. Available: http://homepages.laas.fr/peaucell/software/sdmguide.pdf
[40] Z. Sheng, H. D. Tuan, A. A. Nasir, T. Q. Duong, and H. V. Poor, "Power allocation for energy efficiency and secrecy of wireless interference networks," *IEEE Trans. Wirel. Commun.*, 2018 (Early Access).

Ali Arshad Nasir (S'09-M'13) is an Assistant Professor in the Department of Electrical Engineering, King Fahd University of Petroleum and Minerals (KFUPM), Dhahran, KSA. Previously, he held the position of Assistant Professor in the School of Electrical Engineering and Computer Science (SEECS) at National University of Sciences & Technology (NUST), Paksitan, from 2015-2016. He received his Ph.D. in telecommunications engineering from the Australian National University (ANU), Australia in 2013 and worked there as a Research Fellow from 2012-2015. His research interests are in the area of signal processing in wireless communication systems. He is an Associate Editor for IEEE Canadian Journal of Electrical and Computer Engineering.

Hoang Duong Tuan received the Diploma (Hons.) and Ph.D. degrees in applied mathematics from Odessa State University, Ukraine, in 1987 and 1991, respectively. He spent nine academic years in Japan as an Assistant Professor in the Department of Electronic-Mechanical Engineering, Nagoya University, from 1994 to 1999, and then as an Associate Professor in the Department of Electrical and Computer Engineering, Toyota Technological Institute, Nagoya, from 1999 to 2003. He was a Professor with the School of Electrical Engineering and Telecommunications, University of New South Wales, from 2003 to 2011. He is currently a Professor with the School of Electrical and Data Engineering, University of Technology Sydney. He has been involved in research with the areas of optimization, control, signal processing, wireless communication, and biomedical engineering for more than 20 years.

Trung Q. Duong (S'05, M'12, SM'13) received his Ph.D. degree in Telecommunications Systems from Blekinge Institute of Technology (BTH), Sweden in 2012. Currently, he is with Queen's University Belfast (UK), where he was a Lecturer (Assistant Professor) from 2013 to 2017 and a Reader (Associate Professor) from 2018. His current research interests include Internet of Things (IoT), wireless communications, molecular communications, and signal processing. He is the author or co-author of 290 technical papers published in scientific journals (165 articles) and presented at international conferences (125 papers).

Dr. Duong currently serves as an Editor for the IEEE TRANSACTIONS ON WIRELESS COMMUNICATIONS, IEEE TRANSACTIONS ON COMMUNICATIONS, IET COMMUNICATIONS, and a Lead Senior Editor for IEEE COMMUNICATIONS LETTERS. He was awarded the Best Paper Award at the IEEE Vehicular Technology Conference (VTC-Spring) in 2013, IEEE International Conference on Communications (ICC) 2014, IEEE Global Communications Conference (GLOBECOM) 2016, and IEEE Digital Signal Processing Conference (DSP) 2017. He is the recipient of prestigious Royal Academy of Engineering Research Fellowship (2016-2021) and has won a prestigious Newton Prize 2017.

H. Vincent Poor (S'72, M'77, SM'82, F'87) received the Ph.D. degree in EECS from Princeton University in 1977. From 1977 until 1990, he was on the faculty of the University of Illinois at Urbana-Champaign. Since 1990 he has been on the faculty at Princeton, where he is currently the Michael Henry Strater University Professor of Electrical Engineering. During 2006 to 2016, he served as Dean of Princetons School of Engineering and Applied Science. He has also held visiting appointments at several other universities, including most recently at Berkeley and Cambridge. His research interests are in the areas of information theory and signal processing, and their applications in wireless networks, energy systems and related fields. Among his publications in these areas is the recent book *Information Theoretic Security and Privacy of Information Systems* (Cambridge University Press, 2017).

Dr. Poor is a member of the National Academy of Engineering and the National Academy of Sciences, and is a foreign member of the Chinese Academy of Sciences, the Royal Society, and other national and international academies. He received the Marconi and Armstrong Awards of the IEEE Communications Society in 2007 and 2009, respectively. Recent recognition of his work includes the 2017 IEEE Alexander Graham Bell Medal, Honorary Professorships at Peking University and Tsinghua University, both conferred in 2017, and a D.Sc. *honoris causa* from Syracuse University also awarded in 2017.